PHYSICAL REVIEW E **88**, 060401(R) (2013)

Fractographic aspects of crack branching instability using a phase-field model

H. Henry[1,*] and M. Adda-Bedia[2]

[1]*Physique de la Matière Condensée, Ecole Polytechnique, CNRS, 91128 Palaiseau, France*

[2]*Laboratoire de Physique Statistique, Ecole Normale Supérieure, UPMC Paris 6, Université Paris Diderot, CNRS, 24 rue Lhomond, 75005 Paris, France*

(Received 16 July 2013; published 6 December 2013)

A phase-field model of a crack front propagating in a three-dimensional brittle material is used to study the fractographic patterns induced by the branching instability. The numerical results of this model give rise to crack surfaces that are similar to those obtained in various experimental situations. Depending on applied loading configurations and initial conditions, we show that the branching instability is either restricted to a portion of the crack front or revealed through quasi-two-dimensional branches. For the former, the crack front leaves on the main broken surface either aligned or disordered parabolic marks. For the latter, fractography reveals the so called *échelon* cracks showing that branching instability can also induce crack front fragmentation.

DOI: 10.1103/PhysRevE.88.060401 PACS number(s): 62.20.mt, 46.15.−x, 46.50.+a

Since the pioneering work of Griffith [1], there has been dramatic progress in understanding how and where a crack nucleates and propagates in an initially unbroken solid [2,3]. Nonetheless, some fundamental questions remain open such as the physical mechanisms leading to mist and hackle crack surfaces [4–6] or to branching instability [7–12]. For the former there are some hints supported by experiments: nucleation of microcracks ahead of the crack front [13–16] or *microbranching* instabilities [7,11]. For the latter, studies in the framework of linear elasticity fracture mechanics (LEFM) based on both symmetry considerations and energetic criteria have shown that the branching instability cannot occur below a threshold speed of the crack front [17,18]. However, these studies do not allow one to establish a mechanism for the branching instability itself. This is presumably because in LEFM, the process zone in which the dissipation induced by the crack propagation takes place is reduced to a line. As a result any instability mechanism occurring there cannot be predicted [19]. Numerical tools that introduce a spatial extension of the process zone have been developed to overcome this issue. Among them, the phase-field model [20,21] has shown its ability to properly describe crack propagation in various quasistatic and dynamic situations [22–27]. However, it has not yet been confronted directly with experimental results of dynamic fracture which are primarily three dimensional (3D).

The phase-field model of crack propagation is a phenomenological model that describes the growth of a crack as a phase transition between a purely elastic solid and an infinitely soft phase [20,21]. The evolution equation of the phase field is governed by a Ginzburg-Landau type free energy coupled to the stress field through the elastic energy density. This approach can be related to Γ-convergence theory and *nonlocal* damage theory [28]. It has been proven to retrieve many aspects of LEFM for both two- [22–27] and three-dimensional crack propagation [29,30]. For instance, it reproduces the theoretical prediction of the onset of the branching [23,24] and the instability of a single crack front under mixed mode (I + III) loading [29]. In this work, this model is used to simulate three-dimensional instabilities of fast cracks in a brittle material [30] and compare the results to the experimental fractographic patterns [5,7–16]. We first recall briefly the phase-field model and describe the numerical setup. Thereafter, the qualitative behavior of fracture is presented as the propagation speed is increased. The results show that the three-dimensional branching instability can lead to many fractographic patterns observed experimentally, such as echelon cracks [12] or periodic crescent marks [14,15].

The phase-field model relies on the introduction of an auxiliary field φ that varies between 0 and 1 and is coupled to the elastic field such that the material is infinitely soft when $\varphi = 0$ and obeys the laws of linear elasticity in the regions where $\varphi = 1$. The equations for φ and the elastic field derive from the following free energy density:

$$\mathcal{F} = \frac{D}{2}|\nabla\varphi|^2 + hV(\varphi) + g(\varphi)\left[\frac{\lambda}{2}\varepsilon_{ii}^2 + \mu\varepsilon_{ij}^2 - \varepsilon_c\right], \quad (1)$$

where ε_{ij} $(i = x,y,z)$ is the strain tensor; λ and μ are the Lamé coefficients; and D, h, and ε_c are model parameters that govern the phase-field interface width, its energy, and the phenomenological behavior of the model. The function $V(\varphi) = \varphi^2(1-\varphi)^2$ is a double well potential and $g(\varphi) = 4\varphi^3 - 3\varphi^4$ is a coupling function chosen so that the equilibrium configuration of the one-dimensional crack problem is reached when the stress is completely relaxed in the unbroken material [24]. The evolution equations of both the displacement field u_i and φ are written as

$$\rho\partial_{tt}u_i = \frac{\partial}{\partial x_j}\frac{\partial\mathcal{F}}{\partial\varepsilon_{ij}}, \quad (2)$$

$$\tau\partial_t\varphi = \frac{\partial}{\partial x_i}\frac{\partial\mathcal{F}}{\partial(\nabla_i\varphi)} - \frac{\partial\mathcal{F}}{\partial\varphi}. \quad (3)$$

The evolution equation of the displacement field conserves the total (kinetic plus free) energy, while the evolution equation of the phase field guarantees that $\mathcal{F}$ decreases with time. Notice that the kinetic coefficient τ is a measure of the energy dissipation at the crack front and the fracture energy at zero velocity is given by $G_0 = \sqrt{2D}\int_0^1 d\varphi\sqrt{hV(\varphi) + [1-g(\varphi)]\varepsilon_c}$ [23,24]. Finally, the resulting width of the phase-field interface w_φ can be seen as the spatial extension of a process zone.

In the following, the evolution equations (2) and (3) are applied to an infinitely long parallelepiped of linear elastic material subject to a mode I loading (see Fig. 1). The simulations are performed on a sample of size $W = 160$ and

*Corresponding author: herve.henry@polytechnique.edu

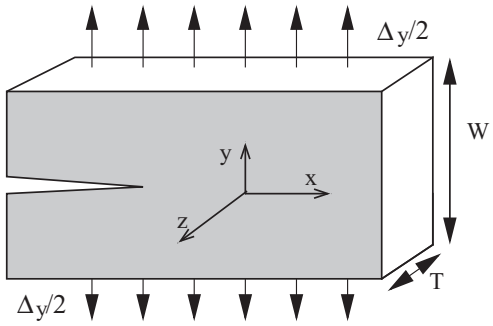

FIG. 1. The simulated setup. A crack front extending along the z axis is propagating along the x axis. Loads are applied through uniform displacements $\pm\Delta_y/2$ at $y = \pm W/2$.

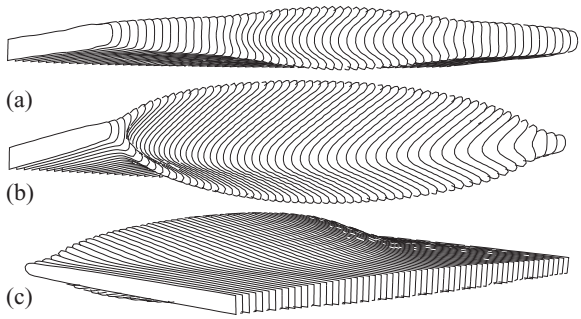

FIG. 2. Perspective view of the isosurface $\varphi = 0.5$ (that can be considered as the crack surface) at different times of a branching event for a thin system ($T \approx 12 w_\varphi$) with traction-free boundary conditions at $z = \pm T/2$. (a) A tip-splitting instability is initiated at the middle of the crack front and (b) spreads along the crack front. (c) represents the same state as (b) seen from the rear crack front.

$T = 120$, density $\rho = 1$, and Lamé coefficients $\lambda = \mu = 1$ corresponding to a Poisson ratio $\nu = 0.25$ and a shear wave speed $c_s = 1$. The following phase-field parameters are used: $D = 2$, $h = 1$, $\varepsilon_c = 1$, and $\tau = 2$ which corresponds to a low dissipation at the crack front [23]. Using these values, one finds $w_\varphi \approx 2$ which is two orders of magnitude smaller than the sizes of the sample W and T. Additional simulations were performed using $D = 4$, $h = 1/2$, and $\varepsilon_c = 1/2$ which keeps fracture energy constant, while w_φ is four times larger. The results display no qualitative changes indicating that scale separation is large enough.

The equations were simulated on a regular tridimensional grid of size $L \times W \times T$ moving along the x axis. As an initial condition, the material was prebroken through a half-plane whose front was slightly perturbed by a sine wave with an amplitude of a few grid points. The crack dynamics is controlled by the imposed displacements $\pm\Delta_y/2$ at $y = \pm W/2$ that also determine the elastic energy per unit surface in the xz plane stored in the intact material, $G = (\lambda/2 + \mu)\Delta_y^2/W$. At the planes $z = \pm T/2$, either periodic or surface-free boundary conditions were used. While the latter breaks translational invariance along the z axis and prevents a purely bidimensional pattern to appear, the former induces a self-interaction of the crack front with itself. To follow cracks over long distances the simulation window was regularly shifted by one grid point in the x direction keeping the most advanced point of the crack front close to the center of the grid [24]. At $x = -L/2$, displacements were inherited from the previous grid shift and at $x = L/2$, they were $u_x = u_z = 0$ and $u_y = y\Delta/W$. To avoid wave reflection at $x = L/2$, damping in Eq. (2) was introduced close to this boundary through a $-\eta\dot{\mathbf{u}}$ term. We checked that this does not affect the crack dynamics by considering systems with different lengths L ($2W$ and $4W$). During simulations, the position of the crack front and the shape of the crack surface were recorded.

Let us now turn to the description of numerical results. At low crack speeds, the crack front propagates at constant speed by keeping its location in the plane $y = 0$. At least for the parameters used here, the crack front does not exhibit any dynamic instability and the crack surfaces are always mirrorlike. When the crack speed is increased above a threshold value that depends on dissipation and model parameters [23], the propagation of a single crack becomes unstable both in the two-dimensional and three-dimensional cases: through a tip-splitting instability, the crack front branches into two cracks that further propagate until the speed of one crack becomes faster and screens the slower one [23,24]. In the three-dimensional case, the nature of the instability is similar but the translational invariance along the crack front is broken, leading to various patterns that are described below. One should note that while in two dimensions, the threshold crack tip speed for branching is well determined, the local character of the instability prevents its accurate computation in the three-dimensional case. Before analyzing the fractography of the broken surface induced by branching instability, the single branching event will be described in detail.

Figure 2 shows the development of a branching event in a thin plate ($T \approx 12 w_\varphi$) slightly above threshold. In this case, the crack front starts to branch locally in the z direction, then the region where splitting occurs grows along the crack front until one of the branches stops and a single crack propagation regime resumes. While this behavior is not surprising in the case of a sample of finite thickness, it is also observed in the case of periodic boundary conditions long after the initial branching event.

For samples of larger thickness, the branching instability also occurs locally on the crack front and the successive branching events follow the scenario described above. Figure 3 shows a typical example of this situation in which branches do not spread through the whole z direction and tend to align along the main direction of crack propagation. This branching pattern is reminiscent of experimental observations where a roughly periodic structure, which is approximately in phase with the crack velocity oscillations, is formed [9–11]. Our results allow one to correlate branching instability with local instantaneous velocity of the crack front and give some rationale for the existence of aligned branching events. Figure 3 shows that once a branching event has occurred, the crack front slows down at the branching point while the rest of the front is not perturbed. The subsequent evolution leads to the formation of a cusped V shape which accelerates after the branching event is finished in order to recover a flat crack front. This implies that the local speed is more likely above the threshold velocity for branching and thus the next branching event occurs at the same position along the crack front. The propagation of elastic waves introduces some randomness in the system and prevents this deterministic branching scheme from repeating

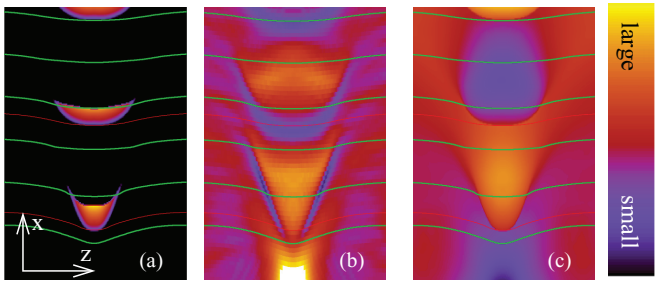

FIG. 3. (Color online) xz contour plots of crack front dynamics and fractography of the resulting surface near the instability threshold. A window of the total fracture surface ($0.2\,T$ in the z direction and $0.375\,T$ in the x direction) is shown. In (a) branching events are displayed: the black region corresponds to a single crack front phase. Elsewhere the distance in the y direction between the two propagating fronts is shown. In (b) the local instantaneous crack front velocity of the most advanced front is plotted showing that the crack front dynamics is correlated with branching instability. The crack front slows down locally before nucleation of a branching event (purple V marks) and accelerates after the arrest of the secondary branch. (c) Shape of the postmortem fracture surface. The height of the crack surface oscillates around the mean position $y = 0$. In all figures, lines display instantaneous positions of the front in the single crack propagation phase.

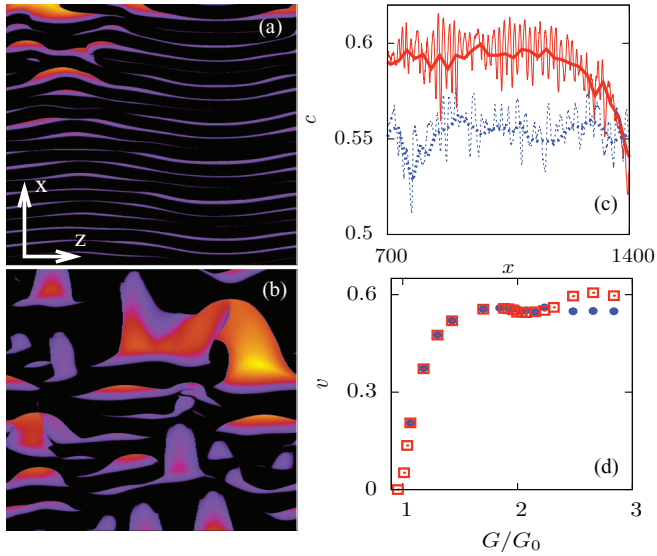

FIG. 4. (Color online) (a), (b) Two fracture morphologies obtained using different initial perturbations of the crack front. The color plots use the same representation of branching as in Fig. 3(a). In (a) branching spreads through the thickness of the sample, while in (b) there are localized and disordered branching events. (c) The instantaneous speeds averaged along the crack front corresponding to cases (a) (thin red line) and (b) (thin blue line). Thick lines are the corresponding average velocities v along a moving time window of size 20. The velocity of quasi-bidimensional pattern (a) is significantly larger than that of 3D pattern (b). The decrease observed at the end of the signal corresponds to a transition to 3D localized branching events and further evolution of the crack propagation leads to a pattern similar to (b). (d) Average velocity of the crack front v as a function of G/G_0, the ratio of the available elastic energy and the fracture energy. □, results of 2D simulations [23]; and •, results from actual 3D simulations.

indefinitely. Figure 3(c) shows that each branching event gives rise to a vertical deformation of the main crack surface that persists over a distance longer than the branching event itself. The induced pattern on the crack surface is similar to parabolic marks observed in experiments [13–16] with the significant difference that the phase-field simulations do not resolve scales smaller than w_φ, while experimental observations are made at the actual scale of the process zone. Nevertheless, the question whether this similarity persists when w_φ is diminished by a few orders of magnitude remains open.

When the crack speed is further increased, one observes a large variety of patterns that appear to be due to the sensitivity to initial conditions and to disorder. Indeed, in some situations, branching events spread through the whole width of the sample and give rise to a branching pattern that is very similar to the one observed in two dimensions [see Fig. 4(a)]. Nonetheless, this is mostly observed when the thickness T is small. In the case of thick samples ($T \gg w_\varphi$), these quasi-bidimensional structures are rarely observed and the most frequent pattern is an apparently disordered array of branching events with varying amplitude and thickness [see Fig. 4(b)]. Quasi-bidimensional patterns tend also to undergo a transition toward the fully tridimensional ones after a sufficiently long crack propagation. When considering the average velocity of cracks this difference in the nature of the patterns (3D or 2D) translates into the fact that cracks with quasi-bidimensional structures have higher average velocities than cracks with three-dimensional branching patterns [see Fig. 4(c)]. This is in qualitative agreement with the fact that the total crack surface is significantly higher in the case of three-dimensional patterns: The difference in crack surface between the samples of Figs. 4(a) and 4(b) is approximately 20%. Indeed, this increase in crack surface can be seen as an additional energy dissipation at the crack tip, leading to crack slowdown. Figure 4(d) confirms that for a finite range of G/G_0 corresponding to a regime where patterns similar to Fig. 4(b) are formed, the velocity measured during 3D simulations is significantly smaller than the one measured for 2D simulations. The measurements of both the energy flux into the front of the moving crack at a given speed and the total surface area created via the microbranching instability show that the instability is the main mechanism for energy dissipation by a moving crack in brittle materials.

Finally, it should be mentioned that in some simulations the interplay of disordered branching events leads to the birth of structures that are reminiscent of the so called *échelon cracks*. These are two cracks propagating in the same direction but on different planes separated by a discontinuity in the crack surface. Indeed, in some circumstances, two distinct planar cracks were propagating parallel to each other (see Fig. 5). The distance over which the echelon cracks persist is much larger for the case of traction-free surface boundary conditions than for the case of periodic boundary conditions. This difference can be attributed to the self-interaction of a crack with itself that is induced by periodic boundary conditions. Hence under pure mode I loading, the localized branching event can induce front fragmentation similarly to what is observed under mixed mode (I + III) loading [29,31,32].

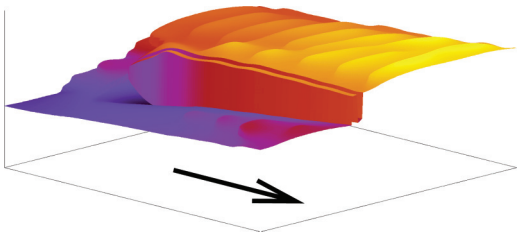

FIG. 5. (Color online) A fracture surface with an echelon crack. The whole thickness of the material is shown and the secondary branches have been removed for clarity. Traction-free boundary conditions at $z = \pm T/2$ were used in the simulation. The arrow indicates the main direction of crack propagation.

The existence of various morphologies within the same loading conditions leads to the question of pattern selection by the system. As shown in Figs. 4(a) and 5, one can see that during the crack propagation the nature of the pattern can change. In both cases, the *transition* is first local and then spreads through the sample as the crack propagates. Second, the introduction of quenched disorder in the system, such as a random variation of the kinematic coefficient of the phase field τ, strongly favors the three-dimensional pattern.

To conclude, the fast propagation of cracks was simulated in three dimensions. As expected, the branching instability was observed and, even in a homogeneous system, one could observe the birth of three-dimensional patterns. These patterns were induced by a sole instability mechanism: a tip-splitting instability of the crack front. Neither crack nucleation nor sidebranching (where a secondary crack nucleates at the surface of an existing crack) were observed. The patterns found reproduce qualitatively various experimental fractographic observations, despite the simplicity of the description of the breaking process in the phase-field model. This indicates that the details of the breaking mechanism in the process zone may play a limited role in the *formation* of fractographic patterns. It is also fairly remarkable that for a given parameter set, depending on the initial conditions and the position along the crack propagation axis, different patterns are observed. These results show that the phase-field model is a valuable tool to study in depth the statistical aspects of dynamical and morphological instabilities of cracks and is a strong argument in favor of the use of diffuse interface approaches to model crack propagation. For instance, the use of advanced computational techniques will allow one to consider larger systems where finite size effects introduced by the phase-field approach can be quantified.

[1] A. A. Griffith, Philos. Trans. R. Soc. A **221**, 163 (1921).
[2] L. B. Freund, *Dynamic Fracture Mechanics* (Cambridge University Press, Cambridge, England, 1990).
[3] J. Fineberg and M. Marder, Phys. Rep. **313**, 1 (1999).
[4] E. Bouchaud, J. P. Bouchaud, D. S. Fisher, S. Ramanathan, and J. R. Rice, J. Mech. Phys. Solids **50**, 1703 (2002).
[5] K. Ravi-Chandar, Int. J. Fract. **90**, 83 (1998).
[6] D. Hull, *Fractography* (Cambridge University Press, Cambridge, England, 1999).
[7] K. Ravi-Chandar and W. G. Knauss, Int. J. Fract. **26**, 141 (1984).
[8] J. Fineberg, S. P. Gross, M. Marder, and H. L. Swinney, Phys. Rev. Lett. **67**, 457 (1991).
[9] E. Sharon, S. P. Gross, and J. Fineberg, Phys. Rev. Lett. **74**, 5096 (1995).
[10] E. Sharon, S. P. Gross, and J. Fineberg, Phys. Rev. Lett. **76**, 2117 (1996).
[11] E. Sharon and J. Fineberg, Phys. Rev. B **54**, 7128 (1996).
[12] A. Sagi, J. Fineberg, and Z. Reches, J. Geophys. Res. **109**, B10209 (2004).
[13] K. Ravi-Chandar and W. G. Knauss, Int. J. Fract. **26**, 65 (1984).
[14] K. Ravi-Chandar and B. Yang, J. Mech. Phys. Solids **45**, 535 (1997).
[15] J. Scheibert, C. Guerra, F. Célarié, D. Dalmas, and D. Bonamy, Phys. Rev. Lett. **104**, 045501 (2010).
[16] C. Guerra, J. Scheibert, D. Bonamy, and D. Dalmas, Proc. Natl. Acad. Sci. USA **109**, 390 (2012).
[17] M. Adda-Bedia, J. Mech. Phys. Solids **53**, 227 (2005).
[18] E. Katzav, M. Adda-Bedia, and R. Arias, Int. J. Fract. **143**, 245 (2007).
[19] E. Bouchbinder, J. Fineberg, and M. Marder, Annu. Rev. Condens. Matter Phys. **1**, 371 (2010).
[20] A. Karma, D. A. Kessler, and H. Levine, Phys. Rev. Lett. **87**, 045501 (2001).
[21] I. S. Aranson, V. A. Kalatsky, and V. M. Vinokur, Phys. Rev. Lett. **85**, 118 (2000).
[22] H. Henry and H. Levine, Phys. Rev. Lett. **93**, 105504 (2004).
[23] H. Henry, Europhys. Lett. **83**, 16004 (2008).
[24] A. Karma and A. E. Lobkovsky, Phys. Rev. Lett. **92**, 245510 (2004).
[25] R. Spatschek, M. Hartmann, E. Brener, H. Muller-Krumbhaar, and K. Kassner, Phys. Rev. Lett. **96**, 015502 (2006).
[26] R. Spatschek, E. Brener, and A. Karma, Philos. Mag. **91**, 75 (2011).
[27] V. Hakim and A. Karma, J. Mech. Phys. Solids **57**, 342 (2009).
[28] B. Bourdin, G. A. Francfort, and J. J. Marigo, J. Mech. Phys. Solids **48**, 797 (2000).
[29] A. J. Pons and A. Karma, Nature (London **464**, 85 (2010).
[30] H. Henry, Europhys. Lett. **92**, 46002 (2010).
[31] D. D. Pollard, P. Segall, and P. T. Delaney, Geol. Soc. Am. Bull. **93**, 1291 (1982).
[32] T. Baumberger, C. Caroli, D. Martina, and O. Ronsin, Phys. Rev. Lett. **100**, 178303 (2008).